

## Non-equilibrium processes in martensitic phase transformations by X-ray photon correlation spectroscopy

Michael Widera<sup>1</sup> and Uwe Klemradt<sup>1</sup>,

<sup>1</sup>2<sup>nd</sup> Institute of Physics and JARA-FIT, RWTH Aachen University, D-52056 Aachen, Germany.

### ABSTRACT

Through undulator sources at 3<sup>rd</sup> generation synchrotrons, highly coherent X-rays with sufficient flux are nowadays routinely available, which allow carrying over photon correlation spectroscopy (PCS) from visible light to the X-ray regime. X-ray photon correlation spectroscopy (XPCS) is based on the auto-correlation of X-ray speckle patterns during the temporal evolution of a material and provides access both to equilibrium and non-equilibrium properties of materials at the Angstrom scale. Owing to technical limitations (detector readout), XPCS has typically been used for the detection of slow dynamics on the scale of seconds. The variety of scattering geometries employed in conventional X-ray analysis can be combined with XPCS. In this work, we report on bulk diffraction (XRD) used to study the prototypical shape memory alloy Ni<sub>63</sub>Al<sub>37</sub> undergoing a structural, diffusionless (martensitic) transformation. Two-time correlation functions reveal non-equilibrium dynamics superimposed with microstructural avalanches.

### INTRODUCTION

The shape memory effect is based on a diffusionless, structural (martensitic) phase transition. Although shape memory alloys are key functional materials with considerable use in technical applications, the underlying transformation mechanism is still little understood. Being of first order, the martensitic transition (MT) proceeds by nucleation and growth. However, typically the transition is only weakly of first order, e.g. with a small latent heat and accompanied by a hysteresis width on the order of about 10 K. Owing to the reduced symmetry of the low temperature phase, typically several variants (domains) of the martensitic phase are nucleated on cooling. Although these possess the same structure, the variants are nucleated with different orientations (unless prevented by some biasing field). This leads to the buildup of twin-related variants and self-accommodation in order to minimize strain. Since the variants are related to each other by orientation relations, which can be considered compatibility relations of the self-accommodation process, the MT necessarily involves the temperature-dependent up-folding of a surface relief [1, 2]. In contrast to steel, the MT in shape memory alloys appears to be close to a second order phase transition. Precursor effects that herald the new phase well above the actual transition temperature are frequently observed, for example pronounced phonon softening [3-5] in neutron scattering, anomalous elastic constants in ultrasound experiments [6] and tweed patterns observed in transmission electron microscopy [1]. By definition, a prototypical MT proceeds without diffusion [7]. This explains why largely athermal transformations are observed, where the amount of material transformed depends solely on the degree of undercooling, and the conversion of the high temperature phase progresses with nearly the speed of sound, even at temperatures below 100 K. Of course, diffusion is unavoidable at finite temperatures, but is considered not to be a key ingredient of MT. However, there are effects in MT that have been attributed to diffusion superimposed on an essentially diffusionless

transformation, in particular ageing effects on long time scales (minutes to hours) [8]. The latter were attributed to short-range diffusion after a change of local symmetry resulting from a MT (“symmetry conforming short-range order”, SC-SRO) [9].

Using 3<sup>rd</sup> generation synchrotron radiation sources, it has become possible to access slow dynamics on the microscopic scale with coherent X-rays. The use of coherent photons had led to novel investigation techniques such as X-ray Photon Correlation Spectroscopy (XPCS), which tracks down time-dependent phenomena in soft and solid condensed matter systems. Using coherent X-ray beams, the individual arrangement of scatterers in real crystals can be shown through a grainy diffraction pattern, also called “speckle” pattern. If the individual arrangement of scatterers changes over time, also the speckle pattern changes and time-dependent intensity fluctuations are observable [10]. The resulting time-dependent evolution of a speckle pattern for equilibrium dynamics can be analyzed using the one-time correlation function (CF) [11]

$$g^{(2)}(\vec{Q}, \tau) = \frac{\langle I(\vec{Q}, t) \cdot I(\vec{Q}, t + \tau) \rangle_\tau}{\langle I(\vec{Q}, t) \rangle_\tau \cdot \langle I(\vec{Q}, t + \tau) \rangle_\tau}, \quad (1)$$

where  $\langle \dots \rangle_T$  denotes an average over time. The zero-point in time is not significant, since only the time difference  $\tau = t_2 - t_1$  enters Eq. (1). Typically, one-time CFs show little change for short time lags  $\tau$ , but drop drastically in the long run. Experimentally determined CF are frequently parameterized as stretched exponentials, e.g. Kohlrausch-Williams-Watts (KWW) functions [10]

$$g^{(2)} = 1 + A \cdot \exp(-2[\tau/\tau_0]^\beta). \quad (2)$$

The stretching exponent  $\beta$  can be different from one, with the numerical value being amenable to physical interpretation: a decay faster than exponential ( $\beta > 1$ ) is associated with solid-like, collective dynamics, a slower decay ( $\beta < 1$ ) with liquid-like, diffusional dynamics [12].

In the case of non-equilibrium systems, the evolving dynamics cannot be meaningfully tracked by the one-time CF. Instead, a two-time CF is more appropriate [13]:

$$C(t_1, t_2) = \frac{\langle I(t_1) \cdot I(t_2) \rangle - \langle I(t_1) \rangle \langle I(t_2) \rangle}{\left( \langle I^2(t_1) \rangle - \langle I(t_1) \rangle^2 \right)^{1/2} \left( \langle I^2(t_2) \rangle - \langle I(t_2) \rangle^2 \right)^{1/2}}, \quad (3)$$

where  $\langle \dots \rangle$  denotes an average over pixels from a region of interest (ROI), making  $C(t_1, t_2)$  also a function of the corresponding wave vectors  $\vec{Q}$ . Note that in contrast to Eq. (1), in Eq. (3) the zero-point in time now has acquired physical meaning. The average time after start of the experiment,  $\bar{t} = \frac{1}{2}(t_1 + t_2) =: t_{age}$ , is a convenient measure of the age of the evolving system. This coordinate corresponds in  $C(t_1, t_2)$  diagrams to the diagonal from the lower left to the upper right corner. A cut along the time-difference coordinate  $\tau = t_2 - t_1$  is perpendicular to that diagonal and provides a characteristic correlation time of the system at  $t_{age}$  [13], in contrast to the correlation time averaged over all system ages, provided by Eq. (1).

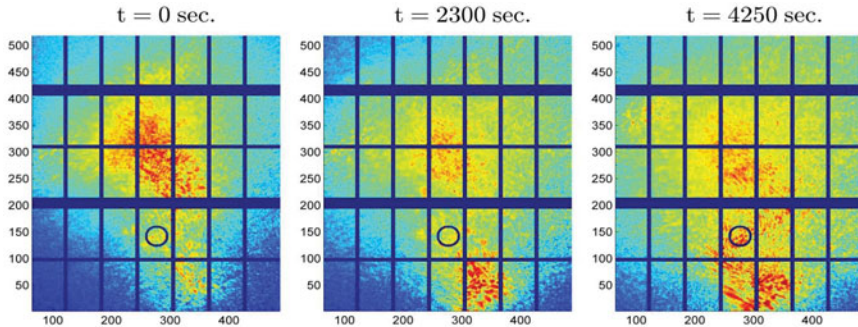


**Figure 1.** Speckle pattern produced with a partly coherent X-ray beam at the (001) reflection in Bragg geometry for a  $\text{Ni}_{63}\text{Al}_{37}$  crystal at 0 s, 2300 s and 4250 s (time series taken under isothermal conditions at  $T = 278.5$  K). The ROI used to calculate the two-time correlation function depicted in Fig. 2 is indicated schematically as a circle. It corresponds to 79 pixels with a radius of approximately  $q_r = 2 \cdot 10^{-3} \text{ \AA}^{-1}$ .

## EXPERIMENTAL DETAILS

For the investigation of slow time-dependent phenomena, a  $\text{Ni}_{63}\text{Al}_{37}$  crystal was investigated using XPCS in diffraction geometry. The single crystal with a (001) polished surface was studied at the coherence beamline P10 of the PETRA III synchrotron at DESY. The experiment was carried out in Bragg geometry using the (001) reflection at  $\Theta_B = 13.51^\circ$  for X-rays of 9.3 keV energy. The undulator beam was focused by compound refractive lenses to a spot size of about  $5 \times 5 \text{ \mu m}^2$  (FWHM) at the sample. The diffracted X-rays were detected by a Pilatus 300K detector ( $487 \times 619$  pixels, pixel size  $172 \times 172 \text{ \mu m}^2$ ) placed 4975 mm downstream of the sample. Various time series of the speckle distribution centered at the (001) reflection were recorded for selected temperatures a few Kelvin above and at the MT, as shown exemplarily in Fig. 1. The temperature stability was ensured by a dedicated setup limiting temperature fluctuations to  $\pm 3$  mK over 24 hrs. Data were taken with an exposure time of 1 sec for intensity reasons, compatible with the focus of the experiment on slow dynamics. The detector readout time was 3 msec.

## RESULTS

As can be seen from the typical data shown in Fig. 1, the speckle pattern at the (001) Bragg reflection undergoes partially strong changes while other areas remain essentially unchanged. We can therefore rule out trivial relaxation processes of the entire sample (e.g., associated with the sample mount etc.) and relate these changes to partial transformations in the sample. It is well known that MTs into the low temperature phase proceed by avalanches, which emit acoustic emission events following power laws [14]. We confirmed the occurrence of avalanches in the samples investigated here independently by acoustic emission spectroscopy.

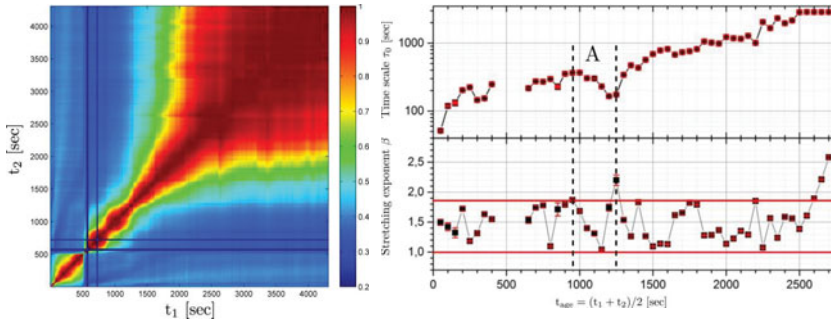


**Figure 2.** (Left) Two-time CF for  $\text{Ni}_{63}\text{Al}_{37}$  at a temperature of 278.5 K. The contours quantify the degree of correlation between the speckle patterns (The two vertical and horizontal lines are artefacts arising from detector readout error). (Right) Characteristic time scales  $\tau_0$  and corresponding KWW exponents  $\beta$  extracted from the two-time CF using non-averaged one-time CF at a given age of the material. The stretching exponent varies repeatedly between 1 and ca. 2, indicating the build-up of internal stress fields that relax temporarily by microstructural avalanches which partially transform the sample.

It should be emphasized that the (001) austenite reflection splits upon the MT due to the lower symmetry of the martensitic phase. Therefore it appears reasonable to relate time-dependent changes of the associated speckle pattern to the phase transformation. More specifically, since the origin of speckle is disorder, a given speckle pattern is closely related to the exact spatial arrangement of the scatterers [11]. Metallic single crystals usually exhibit fairly broad Bragg reflections when measured with incoherent X-rays, hence the corresponding speckle pattern contains information on a variety of related defects. These include (small-angle) grain boundaries separating the mosaic blocks, but also atomic defects, which give rise to Huang scattering around Bragg spots in conventional X-ray scattering [15]. This effect is particularly present in shape memory alloys, for example in  $\text{Ni}_{63}\text{Al}_{37}$  due to the excess nickel [16]. The diffusionless transformation proceeds locally on the order of the speed of sound, so avalanches take extended arrays of unit cells from cubic to tetragonal or orthorhombic symmetry. This changes drastically the exact spatial arrangement of scatterers, which must result in sudden jumps of the related parts of the speckle pattern on the time scale of the experiment.

These features are mirrored by Fig. 2, showing the two-time CF of the ROI from Fig. 1, calculated using Eq. (3). The degree of correlation between the speckle patterns is scale-coded, with higher values representing stronger correlations. The results presented here are essentially independent of the particular choice of the ROI. The local  $M_s$  temperature of the spot under investigation was determined to be  $M_s = 278.5$  K, since at this temperature the speckle pattern changed dramatically, indicating massive structural rearrangement. To ensure a rather complete record of the non-equilibrium dynamics, a time series extending over more than 4000 seconds had been taken. Two major aspects should be pointed out:

First, the time evolution of the speckle pattern shows occasional jerky movements, mirrored by sharp cuts (breakdowns) of the two-time CF. We attribute these findings to microstructural avalanches, in accordance with the physics of the system and similar to features in previous XPCS measurements of the MT in gold-cadmium [17] and cobalt [18].

Second, as mentioned in the introduction, a system age can be defined via  $t_{\text{age}} = (t_1 + t_2)/2$ , which corresponds to the diagonal from the lower left to the upper right corner. For non-equilibrium dynamics which relaxes into a steady or even equilibrium state, also the characteristic time scale  $\tau_0$  must evolve over time. The corresponding increase of the correlation time is clearly visible in Fig. 2 (left) as diverging contours. To quantify the evolving dynamics at a given system age, the one-time CF at that particular age was determined using fits of a KWW function (Eq. (2)). The results obtained are shown in Fig. 2 (right), indicating that the stretching exponent  $\beta$  drops repeatedly from values close to 2 to values near 1 (see for example Fig. 1 interval A with  $\beta \sim 1.8$  to  $\beta \sim 1.1$ ). We interpret these findings as follows: larger avalanches passing through or near the illuminated volume are comparatively rare events, which are reflected in occasional collapses of the CF. However, owing to the underlying power law distribution, smaller avalanches occur much more often. Far-reaching strain fields still modify atomic positions in the illuminated volume, which do not lead to collapses but modify the CF quantitatively. In addition, slow atomic rearrangements are expected to take place following an avalanche that takes the austenite phase locally into the martensitic phase [9,19]. As detailed in the established SC-SRO model for ageing in shape memory alloys, the symmetry of the configuration of lattice imperfections both in the austenite and the martensitic state should conform to the crystal symmetry under equilibrium conditions. However, after a sudden change of symmetry brought about by a diffusionless transformation (e.g., the avalanches comprising a MT), the previous local configuration is inherited by the unit cells of the martensitic phase, where this configuration gradually changes into the stable one by atomic rearrangement or relaxation [9], or in other words by short-range diffusion. Exactly this behavior is reflected by Fig. 2 (right): repeatedly, the system dynamics in the illuminated volume changes between a stretching exponent  $\beta \approx 1$  (interpreted as a signature of diffusional dynamics) and values far above 1 (interpreted as signatures of collective behavior). Hence, the physical picture corroborated here is that of microstructural avalanches building up locally stress in the sample, which is relaxed by further avalanches followed by short-range atomic rearrangements.

## CONCLUSIONS

XPCS can provide previously not accessible information for time-dependent phenomena in martensitic transformations. For a  $\text{Ni}_{63}\text{Al}_{37}$  shape memory alloy investigated here, we find at the transition signatures of microstructural avalanches as well as non-equilibrium features on long time scales, in accordance with the macroscopic observation of isothermal ageing. Fits of Kohlrausch-Williams-Watts functions to non-averaged one-time correlation data exhibit solid-like dynamics ( $\beta \gg 1$ ), with  $\beta$  dropping to 1 after stress relaxation by avalanches. This value indicates local atomic rearrangements (short-range diffusion) as suggested by the symmetry-conforming short-range order model.

## REFERENCES

- [1] Z. Nishiyama, *Martensitic Transformation* (Acad. Press New York, 1978).
- [2] T. Davenport, L. Zhou and J. Trivisonno. *Phys. Rev. B* **59**, 3421 (1999).
- [3] S.M. Shapiro, J.Z. Larese, Y. Noda, S.C. Moss and L.E. Tanner. *Phys. Rev. Lett.* **57**, 3199 (1986).

- [4] L. Manosa, A. Planes, J. Zarestky, T. Lograsso, D.L. Schlagel and C. Stassis. *Phys. Rev B* **64**, 024305 (2001).
- [5] T. Ohba, S. Raymond, S.M. Shapiro and K. Otsuka. *Appl. Phys.* **37**, 64 (1998).
- [6] N. Rusovic and H. Warlimont. *Phys. Stat. Sol A* **44**, 609 (1977).7
- [7] M. Cohen, G.B. Olson and P.C. Clapp. Proc. of the International Conference on Martensitic Transformations ICOMAT-79, Ed. W.S. Owen (MIT, Cambridge, 1979).
- [8] K. Nakajima, S. Aoki, K. Otsuka and T. Ohba. *Mat. Lett.* **21**, 271 (1994).
- [9] X. Ren and K. Otsuka. *Nature* **389**, 579 (1997).
- [10] A. Madsen, R.L. Leheny, H. Guo, M. Sprung and O. Czakkel. *New J. of Phys.* **12**, 055001 (2010).
- [11] G. Grübel, A. Madsen and A. Robert. *Soft Matter Characterization*, chapter 13. Springer Science+Business Media, LCC, New York (2008).
- [12] O.G. Shpyrko, E.D. Isaacs, J.M. Logan, Yenjun Feng, G. Aepli, R. Jaramillo, H.C. Kim, T.F. Rosenbaum, P. Zschack, M. Sprung, S. Narayanan and A.R. Sandy. *Nature* **447**, 68 (2007).
- [13] A. Malik, A.R. Sandy, G.B. Stephenso, S.G.J. Mochrie, I. McNulty and M. Sutton. *Phys. Rev. Lett.* **81**, 5832 (1998).
- [14] E. Vives, J. Ortin, L. Manosa, I. Rafols, R. Perez-Magrane, and A. Planes, *Phys. Rev. Lett.* **72**, 1694 (1994).
- [15] M. A. Krivoglaz, *Theory of X-ray and Neutron Scattering by Real Crystals* (New York: Plenum Press, 1969).
- [16] I.M. Robertson, *Phil. Mag. A* **64**, 577 (1991).
- [17] L. Müller, M. Waldorf, C. Gutt, G. Grübel, A. Madsen, T.R. Finlayson, and U. Klemradt, *Phys. Rev. Lett.* **107**, 105701 (2011).
- [18] C. Sanborn, K.F. Ludwig, M.C. Rogers and M. Sutton. *Phys. Rev. Lett.* **107**, 015702 (2011).
- [19] K. Otsuka and X. Ren. *Mat. Sci. Eng A* **312**, 207 (2001).